ACS Macro Letters

Letter

pubs.acs.org/macroletters

Microgel-Based Thermosensitive MRI Contrast Agent

Xinwei Zheng,† Junchao Qian,† Fei Tang, Zengrong Wang, Chunyan Cao, and Kai Zhong*

High Magnetic Field Laboratory, CAS Center for Excellence in Brain Science, Chinese Academy of Sciences, Hefei 230031, P. R. China

Supporting Information

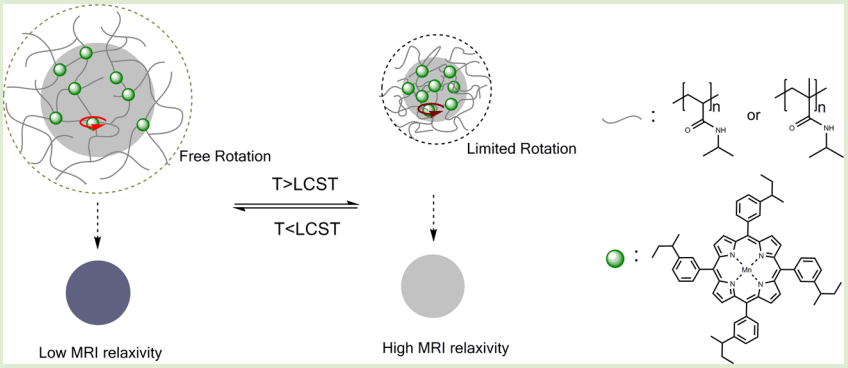

ABSTRACT: Monitoring subtle temperature changes noninvasively remains a challenge for magnetic resonance imaging (MRI). A temperature-sensitive contrast agent based on thermosensitive microgel is proposed and synthesized using a manganese tetra(3-vinylphenyl) porphyrin core reacting with *N*-isopropylacrylamide (NIPAM) or *N*-isopropylmethacrylamide (NIPMAM) monomers and *N*,*N*′-methylenebis(acrylamide) (MBA) cross-linkers. The volume of the NIPAM-incorporated microgel (**M-1**) decreased sharply around its lower critical solution temperature (LCST, 29−33 °C), whereas the volume of the NIPMAM-incorporated microgel (**M-2**) decreased gradually. MR longitudinal relaxivity (r_1) enhancement (44%) was obtained for **M-1**, while the corresponding change for **M-2** was much smaller. **M-1** was further optimized in synthesis without an MBA cross-linker to obtain **M-3** which showed a 67% increase in r_1 around its LCST. Our results suggested that the longitudinal relaxivity is strongly modulated by microgel volume change around the LCST, leading to a significant increase in r_1. This novel thermally sensitive microgel could potentially be applied to monitor small temperature changes using MRI methods.

Noninvasive temperature monitoring with magnetic resonance imaging (MRI) has attracted interest due to the rapid development of thermotherapy.[1,2] Several MRI methods have been proposed to map temperature in phantoms and *in vivo* based on the changes of the longitudinal relaxation time (T_1), the diffusion coefficient, or the proton resonance frequency (PRF).[3−8] Recently, chemical exchange saturation transfer (CEST) agents and spin transition molecular materials[9−13] have also been proposed for temperature measurement. Methods based on spin resonance or spin transfer require a frequency reference to determine the absolute temperature changes. In contrast, temperature changes can be directly deduced from relaxivity measurement using contrast agents. Studies by Fossheim's group explored gadolinium contrast agents entrapped in liposome where longitudinal relaxivity is significantly increased around the liposome phase transition temperature.[14,15] On the other hand, the application is limited due to the leakage of contrast agents from the liposomes. Therefore, a new strategy is required for the development of relaxivity based temperature-sensitive contrast agents.

In this study, we try to combine a paramagnetic core with thermally responsive materials that might show unique temperature response. Microgels are one type of well-studied stimuli-responsive materials, formed by a cross-linked three-dimensional network.[16] Poly(alkylacrylamides), specifically poly(*N*-isopropylacrylamide), are the most widely studied material due to their thermal sensitivity.[17] These microgels show a distinctly rapid swelling and shrinking behavior at the lower critical solution temperature (LCST) in aqueous solution. In addition, they have a much better biocompatibility compared to other toxic agents that favored their potential application *in vivo*. This property has been successfully utilized in numerous applications, such as drug delivery, enzyme carriers, chemical separation technique, nanoreactors, biosensors, etc.[18−25] Recently, microgels have also been applied to fluorescence-based temperature probes.[26,27] The temperature-driven swelling/shrinking of the microgel induces the change in the spatial proximity of fluorescence resonance energy transfer (FRET) donors and acceptors inside the microgel and thus modulates FRET efficiency.

Received: January 24, 2015
Accepted: March 31, 2015
Published: April 1, 2015

DOI: 10.1021/acsmacrolett.5b00058
ACS Macro Lett. 2015, 4, 431−435

Despite the large repertoire of microgel applications, there have been up-to-date no demonstrations utilizing microgels as a viable thermally sensitive MRI contrast agent. The purpose of this work is to investigate the viability and potential gains of incorporating paramagnetic contrast agents into thermosensitive microgels. We hypothesized that temperature-sensitive microgel volume change could be translated into the corresponding longitudinal relaxivity change due to the reduction of paramagnetic core motion under microgel shrinkage. The relaxivity of synthesized microgels was systematically investigated at different temperature to evaluate their temperature response property, and the relationship between the microgel volume and the relaxivity was analyzed.

To produce microgel contrast agents, manganese tetra(3-vinylphenyl) porphyrin was reacted with the *N*-isopropylacrylamide (NIPAM) or *N*-isopropylmethacrylamide (NIPMAM) monomer through free radical emulsion polymerization. The tetra(3-vinylphenyl) porphyrin was synthesized using a standard method described in the literature, which was subsequently incorporated with manganese chloride to produce manganese tetra(3-vinylphenyl) porphyrin. Manganese tetra(3-vinylphenyl) porphyrin was reacted with 200 equiv of NIPAM or NIPMAM and 3 equiv of *N*,*N*′-methylenebis(acrylamide) (MBA) cross-linker. Greenish slurry was obtained after heating the reaction at 70 °C for 6 h. The NIPAM microgel (**M-1**) and NIPMAM microgel (**M-2**) were obtained after dialysis and freeze-drying. Successful manganese porphyrin incorporation into microgels was confirmed by UV−vis spectroscopy, which showed a porphyrin characteristic Soret peak at 472 nm and two Q-band peaks at 573 and 609 nm (Figure 1). According to

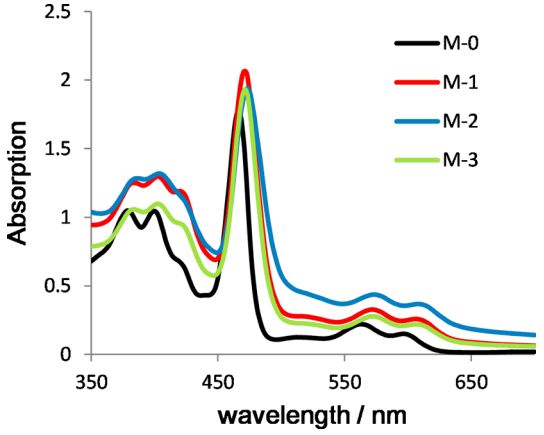

Figure 1. UV−vis spectra of **M-0**, **M-1**, **M-2**, and **M-3**.

the transmission electron microscopy (TEM) images (Figure 2), both **M-1** and **M-2** have a distinct core−shell structure with manganese porphyrin in the inner core and polymer chains forming an outer shell. The average particle sizes of **M-1** and

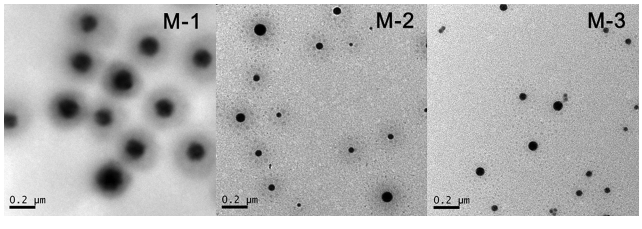

Figure 2. Representative TEM micrographs of **M-1**, **M-2**, and **M-3**.

M-2 at 25 °C were 370 nm (D_{TEM} = 370 nm ± 50 nm) and 240 nm (D_{TEM} = 240 nm ± 110 nm), respectively. In addition, **M-1** with different amounts of manganese porphyrin and sizes could be obtained by varying the ratio of manganese porphyrins to monomers (Table S1, Supporting Information).

Since the manganese tetra(3-vinylphenyl) porphyrin can form four covalent bonds with monomers and acts as a cross-linker itself, we further synthesized NIPAM microgel without the MBA cross-linker to form **M-3**. The preparation of **M-3** was performed by reacting manganese porphyrin with 200 equiv of NIPAM under the indicated conditions. UV−vis spectroscopy showed a similar Soret peak and Q bands compared to that of **M-1** (Figure 1). TEM images of **M-3** showed a clear inner core structure with no polymer outer shell, probably due to the absence of an MBA cross-linker (Figure 2). The average particle size at 25 °C of **M-3** (D_{TEM} = 55 nm ± 25 nm) was much smaller compared to that of **M-1** and **M-2**, with a broader size distribution. Compared to **M-3**, it was obvious from the TEM images that the polymer outer shell contributed a significant portion to the overall particle size for both **M-1** and **M-2**.

The temperature-dependent hydrodynamic diameter of **M-1**, **M-2**, and **M-3** was measured by dynamic light scattering (DLS), with the temperature varied from 25 to 45 °C. The diameter of **M-1** decreased from 530 nm at 25 °C to 320 nm at 45 °C. The majority of changes occurred within a narrow temperature range from 29 to 35 °C, showing a distinctive rapid phase transition. Volume reduction is stabilized above 35 °C, probably due to the fact that the thermosensitive particles were already in the collapsed state. In comparison, **M-2** exhibited a gradual decrease in particle sizes from 350 nm at 25 °C to 300 nm at 39 °C. A phase transition occurred from 39 to 45 °C, and the diameter is further reduced to 210 nm at 45 °C. **M-3** exhibited volume change behavior similar to that of **M-1**, and the phase transition occurred from 27 to 33 °C. The diameter decreased from 128 nm at 27 °C to 97 nm at 33 °C. It is worth noting that for all three nanoparticles the temperature-dependent volume change is completely reversible when the temperature was reversed from 45 °C back to 25 °C. At 25 °C, the diameters of **M-1**, **M-2**, and **M-3** all returned to their original sizes (Figure 3). The LCSTs for **M-1**, **M-2**, and **M-3** were determined as 33, 43, and 31 °C, respectively, from curve fitting (Supporting Information).

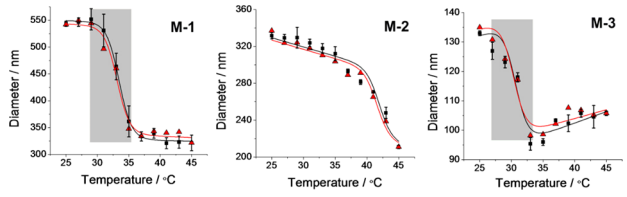

Figure 3. Diameter dependence on temperature for **M-1**, **M-2**, and **M-3**. (sqaure) Heating up and (triangle) cooling down. Red and black lines are fitted curves for corresponding procedures and matched well each other.

To compare the longitudinal relaxivity of the three nanoparticles, we further synthesized water-soluble manganese tetra(4-sulfonatophenyl) porphyrin (**M-0**) as a contrast agent reference. Tetraphenyl porphyrin was reacted with concentrated sulfuric acid at 80 °C to obtain tetra(4-sulfonatophenyl) porphyrin, which was incorporated with manganese chloride to produce **M-0**. The results from UV−vis spectroscopy

DOI: 10.1021/acsmacrolett.5b00058
ACS Macro Lett. 2015, 4, 431−435

confirmed the successful manganese insertion into tetra(4-sulfonatophenyl) porphyrin (Figure 1). As expected, the ^{1}H NMR spectrum of **M-0** was very broad due to the paramagnetic effect of Mn(III) in the porphyrin core (Figure S2, Supporting Information).

The longitudinal relaxivities (r_1) of **M-0** to **M-3** were measured on a 3 T clinical MRI scanner, acquired in a quartz container with four built-in tubes (Figure S1, Supporting Information) and regulated with a circulation pump with ±0.1 °C accuracy. Different agents from **M-0** to **M-3** were measured from 25 to 49 °C. At 25 °C, T_1 enhancement was observed for **M-0**, **M-1**, **M-2**, and **M-3**. Compared to **M-0**, the r_1 values of **M-1**, **M-2**, and **M-3** were smaller at 25 °C. However, the trend is reversed with increased temperature (Figure 4). At 37 °C, the

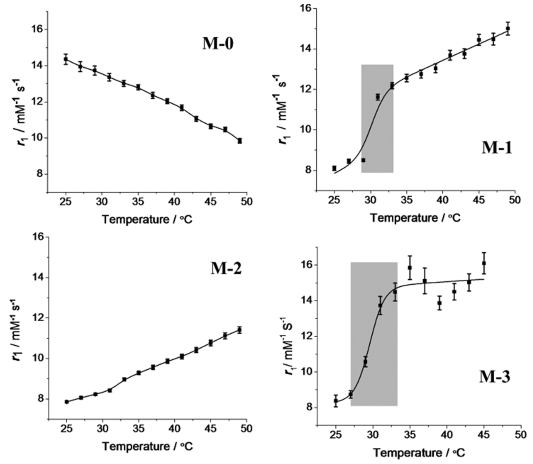

Figure 4. r_1 dependence on temperature for **M-0**, **M-1**, **M-2**, and **M-3**. The r_1 corresponds to the relaxivity per Mn porphyrin.

r_1 of both **M-1** and **M-3** already surpassed that of **M-0**, respectively. Significant r_1 changes were observed for **M-1** and **M-3** in the same temperature ranges that are in good agreement to their corresponding LCST as measured in DLS (gray areas in Figure 3 and Figure 4). **M-1** showed a 44% increase in r_1 around its LCST (8.5 mM^{-1} s^{-1} at 29 °C to 12.2 mM^{-1} s^{-1} at 33 °C). Above 33 °C, the r_1 of **M-1** increased further but is less pronounced and reached 15.0 mM^{-1} s^{-1} at 49 °C. The r_1 of **M-3** increased even more significantly (67%) around its LCST and changed from 8.7 mM^{-1} s^{-1} at 27 °C to 14.5 mM^{-1} s^{-1} at 33 °C. The r_1 of **M-3** is stabilized above 33 °C. In contrast, **M-2** showed a gradual r_1 increase from 7.8 mM^{-1} s^{-1} at 25 °C to 11.4 mM^{-1} s^{-1} at 49 °C. No rapid transition was observed in the **M-2** longitudinal relativity measurement around its LCST. Several characteristics of the synthesized microgel contrast agents and **M-0** are summarized in Table 1.

From DLS and MRI experiments, significant relaxivity increases and rapid volume reduction were observed for the **M-1** and **M-3** over the same temperature range. This consistency of volume change and longitudinal relaxivity change with changing temperature strongly supported our initial hypothesis—that microgel volume change can be translated into the corresponding longitudinal relaxivity change. For both **M-1** and **M-3**, longitudinal relaxation measurement showed a rapid transition around their LCST, while the corresponding TEM images suggested that the outer shell structure is absent for **M-3** compared to that of **M-1**. Therefore, the sharp changes of r_1 at the LCST for both **M-1** and **M-3**

Table 1. Manganese Content, Hydrodynamic Diameter, and Relaxivities of M-0, M-1, M-2, and M-3 Samples

sample	Mn content[a] (wt %)	diameter[b] at 25 °C (nm)	diameter[b] at 37 °C (nm)	r_1 at 25 °C[c] (mM^{-1} s^{-1})	r_1 at 37 °C[c] (mM^{-1} s^{-1})
M-0	7.70	N/A	N/A	14.4 ± 0.3	12.3 ± 0.2
M-1	0.17	530 ± 8	335 ± 7	8.1 ± 0.1	12.8 ± 0.2
M-2	0.14	330 ± 9	290 ± 4	7.9 ± 0.1	9.6 ± 0.1
M-3	0.34	133 ± 1	103 ± 1	8.4 ± 0.3	14.5 ± 0.7

[a]Determined by ICP-AES or ICP-MS. [b]Determined by dynamic light scattering, standard deviation was calculated based on data from three measurements. [c]r_1 corresponds to the longitudinal relaxivity per Mn, and standard deviation was determined through a weighted least-squares regression using a variable flip angle method in MRI T_1 measurement.[28]

could be attributed mainly to the volume reduction of the inner core around the LCST. In comparison, no rapid transition was observed for **M-2** in the relaxivity measurement around its LCST, although significant volume reduction was observed in its DLS measurement from 39 to 45 °C. TEM images suggested that the inner core of **M-2** is much smaller compared to that of **M-1**. Considering that **M-1** and **M-2** were synthesized with similar monomers but differed by one methyl group in the side chain, one might conclude that the hydrophobic interaction played an important role in regulating the size of the inner core. Therefore, the gradual increase in r_1 of **M-2** could be mainly contributed to the volume reduction of the outer shell, which will collapse around its LCST but has a less pronounced effect on the longitudinal relaxation. The effect of the outer shell can also explain the different behavior of r_1 for both **M-1** and **M-3** above their LCST. The r_1 of **M-1** increased steadily above its LCST, while the r_1 of **M-3** stabilized above its LCST due to the absence of the outer shell. Although the outer shell is absence for **M-3**, it clearly showed an expansion/contraction behavior with temperature. This is modulated primarily by the hydrophobic interaction. On the other hand, the absence of the outer shell would further reduce the inner core size and the expansion range of **M-3** with temperature.

Although the inner core and the outer shell both have an effect on the r_1 of **M-1**, **M-2**, and **M-3**, they affected the longitudinal relaxivity in different ways. In the microgel matrix, the longitudinal relaxivity is affected strongly by the rotational correlation time (τ_R) of the paramagnetic core and the water residency time (τ_m) of the coordinated water molecules with paramagnetic core. For a thermally responsive microgel, the inner core volume reduction has a greater impact on τ_R. The reduction in inner core size limited the local mobility of the manganese porphyrin paramagnetic core, due to the steric effects of neighboring functional groups that are more densely packed at higher temperature. This led to an increase in τ_R for manganese porphyrin and concurrently enhanced the longitudinal r_1 around the LCST.

M-2 has a side cross-linking chain with higher hydrophobicity and consequently a small inner core size. Therefore, the change of r_1 would be mainly regulated by the outer shell structure, which affects more τ_m when the outer shell slowly collapses with increasing temperature. Collapse of the outer shell will increase the average retention time of water molecules in the microgel due to the fact that water exchange between bonded water in the microgel and outside free water will be limited by the reduced surface and accessible channels. This will therefore increase the average exchange rate between

DOI: 10.1021/acsmacrolett.5b00058
ACS Macro Lett. 2015, 4, 431−435

coordinated water molecules with water molecules in the microgel. Our measurement with **M-2** showed a steady increase of r_1, while τ_m is decreased with increasing temperature. This suggests that τ_m reduction during outer shell shrinkage would be another source for the longitudinal relaxivity increase. On the other hand, the τ_m effect occurred over a larger temperature range and does not induce a rapid change in longitudinal relaxivity, compared to the effect of τ_R on the inner core.

Interestingly, although **M-0** has a much higher r_1 at 25 °C, its longitudinal relaxivity decreases rapidly and is smaller compared to that of **M-1** and **M-3** above 37 °C. This behavior reflects the difference in relaxation mechanism for small and large paramagnetic molecules. The longitudinal relaxivity of **M-0** is regulated by its τ_R that decreases at higher temperature and reduces the r_1 correspondingly.[29] In comparison, our study found that the longitudinal relaxivity of the thermosensitive microgel is mainly regulated by its inner core and outer shell that increase with temperature. Small paramagnetic contrast agent molecules can usually be modeled as an inner water-bonded core and an outer hydrophilic layer.[30] Therefore, the longitudinal relaxivity of small paramagnetic molecules and large thermosensitive microgels has a similar analogue structure but undergoes different contrast mechanisms. One could tentatively conclude that the understanding of the inner core structure and its behavior is crucial for the development of novel thermomicrogels that can be applied for sensitive temperature mapping with MRI.

Our method with microgel and MR relaxivity is an absolute measurement that employs the intrinsic property of the particle itself, and temperature values can be derived directly from the T_1 measurement. We typically can get a temperature-dependent change in r_1 on the order of 1 mM^{-1} s^{-1} $°C^{-1}$ around the LCST transition region. The typical measurement error in r_1 is around 0.15−0.3 mM^{-1} s^{-1} and is signal-to-noise dependent. This translated to temperature accuracy around 0.15−0.3 °C, which is on par or better than the reported PRF method.[8,31] With better RF coils or even higher field strength, we could expect further SNR increase and higher temperature sensitivity (0.1 °C or better) with the microgel method. Given that the microgel temperature sensitivity is comparable to or better than the PRF method, it could be applied in the future for small MR temperature measurement.

There is literature evidence[32−34] that the LCST transition temperature could be fine-tuned to match the *in vivo* conditions by changing the monomer and comonomer mixture. On the other hand, this needs to be verified for our microgel system. In addition, the changes in monomer and comonomer mixture could lead to different behavior of the microgel in its relaxivity around the LCST. This is certainly a very interesting topic to follow in future studies. Stronger paramagnetic molecules, such as gadolinium, can also be incorporated into the thermosensitive microgel, which could potentially further enhance its performance.

In summary, a feasible approach for preparing thermosensitive microgel contrast agents has been described. The novel contrast agent exhibited significantly r_1 changes over a narrow temperature range and could be used for monitoring of subtle temperature change using MRI.

■ ASSOCIATED CONTENT

Ⓢ Supporting Information

Synthesis of microgels and characterization method are described. This material is available free of charge via the Internet at http://pubs.acs.org.

■ AUTHOR INFORMATION

Corresponding Author

*E-mail: kzhong@hmfl.ac.cn.

Author Contributions

†These authors contributed equally.

Notes

The authors declare no competing financial interest.

■ ACKNOWLEDGMENTS

This work was supported in part by grants from the NNSF of China (U1232212), the National Basic Research Program of China (973 Program 2012CB720704), the NSF of Anhui Province (1208085MH132), and Nurturing Fund of Hefei Physical Science Center (2014FXZY004).

■ REFERENCES

(1) Ludemann, L.; Wlodarczyk, W.; Nadobny, J.; Weihrauch, M.; Gellermann, J.; Wust, P. *Int. J. Hyperthermia* **2010**, *26*, 273−282.
(2) Rieke, V.; Pauly, K. B. *J. Magn. Reson. Imaging* **2008**, *27*, 376−390.
(3) Hey, S.; de Smet, M.; Stehning, C.; Grull, H.; Keupp, J.; Moonen, C. T. W.; Ries, M. *Magn. Reson. Med.* **2012**, *67*, 457−463.
(4) Parker, D. L.; Smith, V.; Sheldon, P.; Crooks, L. E.; Fussell, L. *Med. Phys.* **1983**, *10*, 321−325.
(5) Sakai, K.; Yamada, K.; Sugimoto, N. *NMR Biomed.* **2012**, *25*, 340−346.
(6) Lebihan, D.; Delannoy, J.; Levin, R. L. *Radiology* **1989**, *171*, 853−857.
(7) Liu, G.; Qin, Q.; Chan, K. W. Y.; Li, Y.; Bulte, J. W. M.; McMahon, M. T.; van Zijl, P. C. M.; Gilad, A. A. *NMR Biomed.* **2014**, *27*, 320−331.
(8) Ishihara, Y.; Calderon, A.; Watanabe, H.; Okamoto, K.; Suzuki, Y.; Kuroda, K. *Magn. Reson. Med.* **1995**, *34*, 814−823.
(9) McVicar, N.; Li, A. X.; Suchy, M.; Hudson, R. H. E.; Menon, R. S.; Bartha, R. *Reson. Med.* **2013**, *70*, 1016−1025.
(10) Wu, Y. K.; Evbuomwan, M.; Melendez, M.; Opina, A.; Sherry, A. D. *Future Med. Chem.* **2010**, *2*, 351−366.
(11) Zhang, S. R.; Malloy, C. R.; Sherry, A. D. *J. Am. Chem. Soc.* **2005**, *127*, 17572−17573.
(12) Jeon, I.-R.; Park, J. G.; Haney, C. R.; Harris, T. D. *Chem. Sci.* **2014**, *5*, 2461−2465.
(13) Muller, R. N.; Vander Elst, L.; Laurent, S. *J. Am. Chem. Soc.* **2003**, *125*, 8405−8407.
(14) Fossheim, S. L.; Il'yasov, K. A.; Hennig, J.; Bjornerud, A. *Acad. Radiol.* **2000**, *7*, 1107−1115.
(15) Frich, L.; Bjornerud, A.; Fossheim, S.; Tillung, T.; Gladhaug, I. *Magn. Reson. Med.* **2004**, *52*, 1302−1309.
(16) Pelton, R. *Adv. Colloid Interface Sci.* **2000**, *85*, 1−33.
(17) Guan, Y.; Zhang, Y. J. *Soft Matter* **2011**, *7*, 6375−6384.
(18) Li, P.; Xu, R.; Wang, W.; Li, X.; Xu, Z.; Yeung, K. W. K.; Chu, P. K. *Colloids Surf., B-Biointerfaces* **2013**, *101*, 251−255.
(19) Thorne, J. B.; Vine, G. J.; Snowden, M. J. *Colloid Polym. Sci.* **2011**, *289*, 625−646.
(20) Malmsten, M.; Bysell, H.; Hansson, P. *Curr. Opin. Colloid Interface Sci.* **2010**, *15*, 435−444.
(21) Welsch, N.; Becker, A. L.; Dzubiella, J.; Ballauff, M. *Soft Matter* **2012**, *8*, 1428−1436.
(22) Parasuraman, D.; Serpe, M. J. *ACS Appl. Mater. Interfaces* **2011**, *3*, 2732−2737.

DOI: 10.1021/acsmacrolett.5b00058
ACS Macro Lett. 2015, 4, 431−435

(23) Koda, Y.; Terashima, T.; Sawamoto, M. *Abstr. Pap. Am. Chem. Soc.* **2014**, 246.
(24) Welsch, N.; Ballauff, M.; Lu, Y. *Chem. Des. Responsive Microgels* **2010**, *234*, 129−163.
(25) Sigolaeva, L. V.; Gladyr, S. Y.; Gelissen, A. P. H.; Mergel, O.; Pergushov, D. V.; Kurochkin, I. N.; Plamper, F. A.; Richtering, W. *Biomacromolecules* **2014**, *15* (10), 3735−3745.
(26) Wang, D.; Liu, T.; Yin, J.; Liu, S. *Macromolecules* **2011**, *44*, 2282−2290.
(27) Okada, K.; Maeda, Y. *J. Appl. Polym. Sci.* **2013**, *130*, 201−205.
(28) Cheng, H. L. M.; Wright, G. A. *Magn. Reson. Med.* **2006**, *55*, 566−574.
(29) Caravan, P.; Ellison, J. J.; McMurry, T. J.; Lauffer, R. B. *Chem. Rev.* **1999**, *99*, 2293−2352.
(30) Caravan, P. *Chem. Soc. Rev.* **2006**, *35*, 512−523.
(31) Quesson, B.; de Zwart, J. A.; Moonen, C. T. W. *J. Magn. Reson. Imaging* **2000**, *12*, 525.
(32) Ilboga, S.; Coskun, M. *Polym. Sci., Ser. B* **2014**, *56*, 848−854.
(33) Liu, G.; Li, X.; Xiong, S.; Li, L.; Chu, P. K.; Wu, S.; Xu, Z. *J. Fluorine Chem.* **2012**, *135*, 75−82.
(34) Ma, X. M.; Xing, Y. C. *Polym. Bull.* **2006**, *57*, 207−217.

DOI: 10.1021/acsmacrolett.5b00058
ACS Macro Lett. 2015, 4, 431−435